Volume 1 | Number 1 | Jan 2013 | Pages 1–100

Journal of
Materials Chemistry A

Materials for energy and sustainability
www.rsc.org/materialsA

Li⁺

e⁻

Li⁺

e⁻

Li⁺

Li⁺

ROYAL SOCIETY
OF CHEMISTRY

ROYAL SOCIETY
OF **CHEMISTRY**

www.rsc.org/materialsA

Journal of Materials Chemistry A

ARTICLE

ZnO 1D Nanostructures Designed by Combining Atomic layer deposition and Electrospinning for UV Sensor Applications

Adib Abou Chaaya,[a] Mikhael Bechelany, [a]* Sebastien Balme [a] and Philippe Miele[a]

We explored for the first time the ability of three-dimensional polyacrylonitrile /ZnO material prepared by a low-cost and scalable synthesis method based on the combination of electrospinning and atomic layer deposition (ALD) as new material with large surface area to enhance the performance of UV photodetection. The UV photoresponse current has been enhanced by a factor of 250 compared to a flat electrode. In addition an increase by a factor of 1.3 of the recovery time has been observed which is negligible versus the huge amount of current enhancement. The greatly improved performance and the good stability of these nanostructured electrodes induce exciting materials for their implantation in UV sensor applications.

A Introduction

UV photodetection has been widely studied in the last few years[1-10] due to their large civil and military application fields such as secure space-to-space communications, pollution monitoring, water sterilization, and flame sensing. The semiconductor based UV photodetection process is a simple physical phenomena based on electron-hole generation into a semiconductor under photon shelling. Basically when a photon with energy larger than the one of the semiconductor band-gap is absorbed, an electron-hole pair would be produced. This induces a changing of the electrical conductivity properties of semiconductor. Low band gap energy semiconductors have been widely used for UV photodetection especially the Si-based photodetectors (Eg = 1.1 eV). Despite both their high sensitivity and quick response advantages, low Eg UV photodetectors are sensitive to low energy photons (visible and Infrared), and thus, they require the insertion of protection filters to avoid signal / noise related to those low electron energies. Moreover an ultra-high vacuum and a very high voltage supply were required.[11] The disadvantages of the low Eg based photodetectors disappear for the high band gap semiconductors. Moreover, wide-band gap materials are both chemically and thermally stable which reflects an advantage for devices operating in harsh environments.[12-14] Among the high band gap semiconductor category, ZnO was one of the most used semiconductors for UV photo-detection due to its high chemical stability, low cost, and large band gap of 3.37 eV at room temperature. Mollow *et al.* reports in 1940 the first UV photoresponse in ZnO films.[15] Since then, many complex ZnO-based photodetectors with high performance were reported, such as p-n junction, p-i-n junction and Schottky junction[3, 16-23]. ZnO UV sensors have been prepared using different deposition techniques such as Metal Organic Chemical Vapor Phase Deposition (MOCVD),[24, 25] laser

assisted molecular beam deposition (LAMBD)[26], radio frequency (RF) magnetron sputtering,[27-29] atomic-layer deposition (ALD) [30] and molecular beam epitaxy (MBE).[31, 32] Moreover different electrode types such as Au, Ag, Pt, Ni, Pd, Cr, Al, and Ru have been elaborated and their performances investigated.

Nanostructured ZnO for UV detection was also investigated. They show promising results in term of photoresponse current, rise time and fall time.[33, 34] One dimensional nanostructured (1D NSs) UV photodetectors have attracted attention in the last decade due to their (i) small size, (ii) low cost of fabrication and operation, and (iii) high active surface area combined with the large ability of structural and chemical tuning. Different works have been reported in this field. Wang *et al.* [34] reports the photoconduction mechanism in a ZnO single nanowire. Under UV illumination an electron-hole pair will be generated. Holes migrate to the surface and recombined with the O_2 species adsorbed on the surface, the unpaired electrons are collected at the anode under an applied voltage, which leads to the increasing of the nanowire conductivity. According to Kind *et al.* [33], a transition from a fast photoreponse under oxygen to a slow photoreponse under vacuum assures the oxygen's role. Huang *et al.* [35] reports a three order enhancement on the UV photoreponse of ZnO nanowire due to a polystyrene coating. Lao *et al.* [36] reports a five order magnitude enhancement on the UV photoreponse of ZnO nanobelts due to a surface functionalization with a high UV absorption ability polymer. UV photoreponse was also enhanced by Ag-ZnO nanowire Schottky contact[37]. Aluminium-doped ZnO nanorod arrays were also developed for UV photodetection.[38] According to Suobai *et al.,*[39] the photoresponse current increases linearly with the number of Nanowires (NWs) connected in parallel. A significant improvement on short-term of fast response and recovery times was also reported. Prades *et al.* [40] suggests to decrease the distance between the electrical contacts or

increasing the width of the photoactive area, or improving the electrical mobility of the nanomaterials to enhance ZnO nanowire responses. Lin *et al.* reported a zinc oxide ALD on multiwalled carbon nanotubes for UV photodetector applications [41]. Al-doped ZnO nanorods arrays were also reported by Mamat *et al.* [38] for UV photodetection. Lin *et al.*[42] reported on a photoconductor device that was sensitive to illumination with below-gap light by electrospinning of a single Al doped-ZnO (AZO) nanowire followed by a calcination process at 550°C for 3h to obtain well-aligned polycrystalline AZO nanowires. Shan *et al.* [43] performed a short study on ZnO ALD films deposited on glass substrates for UV photodetection. They show a photoresponse current of ZnO based photodetectors (0.7 AW^{-1} at 5V bias) without the investigation of other parameters such as recovery time, response time and device stability.

In this paper, ZnO 1D NSs based photodetectors are tailored using the atomic layer deposition technique combined with the electrospinning techniques. Polyacrilonitrile fibers synthesized by electrospinning will be used as a template for ZnO ALD deposition in order to enhance the specific surface of the ZnO based UV photodetectors. Structural, chemical and UV photoresponse properties of the obtained materials will be investigated. We should note here that ALD ZnO UV detection was not extensively studied in the literature. The design of high surface electrode based ALD deposition and the investigation of ALD conditions such as temperature and thickness have not been addressed yet.

B Materials and methods

1. Materials

Polyacrylonitrile PAN (M_w = 150000), Dimethylformamide (ACS reagent, $\geq$ 99.8%), and Diethyl Zinc (DEZ) ($Zn(CH_2CH_3)_2$, 95% purity, CAS: 557-20-0) were purchased from Sigma Aldrich.

2. Electrospinning

Starting from a polymer solution, sub-micron nanofibers were synthesized using the electrospinning techniques. The electrostatic field applied between a syringe and a disk collector provides the transformation of the droplet to a Taylor cone. The droplet is stretched under an electrostatic field to form a sub-micron fiber after the evaporation of the solvent.[44] A 60 kV high voltage power supply from ISEG, a Kd Scientific syringe pump, an aluminum collector disk and a glove box were used to build the setup. Electrospinning solution was prepared by dissolving 10 wt. % of polyacrilonitrile in dimethylformamide. The solution was maintained 1 hour under agitation and then heated 20 min at 80°C in an oil bath. The polymer solution was electrospun at room temperature in ambient atmosphere under an applied voltage (25 kV) with a flow rate of 1 mlh^{-1} using a 0.7 mm diameter syringe related to the positive output of the generator. The aluminum disk placed 15 cm from the tip of the syringe was related to the negative output of the generator. 10 x 20 mm glass substrate was fixed on the aluminum disk using carbon tape. Silver glue was used as an ohmic contact on the glass substrate separated by 5 mm distance.

3. Atomic layer deposition of zinc oxide

A custom made ALD reactor was used for the synthesis of ZnO thin films. ALD was performed using sequential exposures of Diethyl Zinc (DEZ) and H_2O separated by a purge of nitrogen with a flow rate of 100 sccm. The deposition regime for ZnO

consisted of a 1.5 s pulse of DEZ, 30 s of exposure to DEZ, 60 s of purge with nitrogen followed by a 3 s pulse of H_2O, 30 s of exposure to H_2O and finally 60 s purge with nitrogen. ZnO thin films with different number of cycles were deposited by varying the temperature from 50 to 130 °C.

4. Structural and chemical characterization

Structural and chemical compositions of all 1D ZnO based NSs were analyzed by scanning electron microscopy (SEM, S-4800, Hitachi), Energy-dispersive X-ray spectroscopy (SEM, S-4500, coupled with a Thermofisher EDX detector), and X-Ray diffraction (PANAlytical Xpert-PRO diffractometer equipped with a X'celerator detector using Ni-filtered Cu-radiation). From the latter the grain size was calculated by Debye-Scherer relationship (Equation 1) (see Supporting Information SI2):

$$D = \frac{0.9 \cdot \lambda}{\beta \cdot cos(\theta)}$$

(Equation1)

5. UV sensor measurement

Characterizations of electrical conductivity of 1D ZnO NSs samples deposited under different conditions were performed under dark and UV illumination in order to study the photodetector properties. Electrodes with a 5 mm distance between the 2 electrodes and a width of 10 mm have been used for this study. The UV detection cell is a homemade cell designed from a black box. A UV source (365 nm, 4W) (Roth, France) has been used for UV illumination. The Radiation intensity of the 365 nm UV illuminated on the device was 80 mW/cm^2. The relative humidity was measured to be 30%.

Both Sweep voltammetry and chronoamperometry measurement have been performed using a potentiostat (from EG&G instruments model 265A). Sweep voltammetry has been measured from -3V and 3V with a scan speed of 50 $mV.s^{-1}$. Chronoamperometry measurement was performed with on/off UV illumination in order to extract the photoresponse current and the recovery time. They have performed at -1V during 3000 seconds using the following protocol (i) UV off between 0 and 100 s, (ii) UV on between 100 and 200 s and (iii) UV off between 200 and 3000 s. From Chronoamperometry experiments, UV photoresponse parameters have been extract: (i) current (ΔI) defined as: $\Delta I = I_{UV} - I_{Dark}$ (where I_{Dark} is current under dark and I_{UV} is the current under UV illumination 365 mn) and (ii) the recovery time (τ), defined as the time for the photoresponse current to drop to 1/e (37%) of the maximum photoresponse current [39]. During the electrical measurement the UV cell was covered with a black box to assure perfect light isolation. We note here that due to the limitation of our device, the responsivity was not extracted and compared in this work.

C Results and discussion

1. Design of 1D ZnO nanostructures

The schematic process for the design of the electrode is reported in Figure 1(a). Figure 1(b) shows the SEM images of 1D ZnO NSs obtained with 240 s of electrospinning time coated with 250 cycles of ALD ZnO at 100°C. These images indicate a conformal coating of the PAN nanofibers obtained by this method. The PAN/ZnO NFs develop a rough surface with lamellar morphology as attested by HRSEM images (see Supporting Information SI: Figure S1 and S2). EDX measurement (not reported here) has been performed on the sample in order to evaluate the chemical composition. The presence of Zn, O and C can be observed. XRD diffraction

(Figure 1c) shows peaks at $2\theta = 31.74°$, $34.42°$ and $36.22°$ respectively corresponding to (100), (002) and (101) of ZnO as generally observed with the ZnO thin films deposited by ALD.[45]
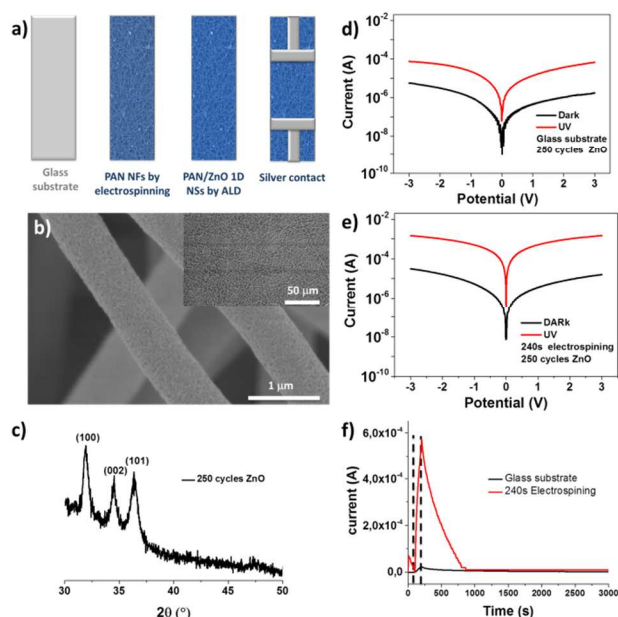

Figure 1. . a) Schema of the design of PAN/ ZnO 1D NSs UV sensor; b) SEM images of 1D ZnO NSs obtained with 240 s electrospinning time coated with 250 cycles ALD ZnO at 100°C c) X-Ray diffraction spectra; Sweep voltammetry of ALD ZnO thin layer (50 nm thick) on Glass (d) and with 240 s electrsopinning time (e); and f) Chronoamperometry measurements of sensors on Glass and with 240 s electrospinning times with UV (365 nm) illumination between 100 and 200 s.

A high-performance photodetector should satisfy the 5S requirements of high sensitivity, high signal-to-noise ratio, high spectral selectivity, high speed and high stability[46]. The sweep voltammetry of ZnO sensors on glass (Figure 1d) and PAN/ZnO 1D NSs confirm a Schottky junction between the ZnO and the Ag contact. As shown in Figure 1d and 1e, measurements exhibit a stable I_{Dark} value 10^{-5}-10^{-6} A at -1V bias on Glass and on PAN electrospun nanofibers. In the contrary, the I_{UV} current increases from 2.26×10^{-6} to 5.7×10^{-4} A. This UV response increment was expected due to the enhancement on the specific area of ZnO 1D NSs exposed to UV light. We note here that due to the low weight of the deposited PAN/ZnO 1D NSs and to the polymer composition of the core of the NSs, Brunauer-Emmett-Teller (BET) experiments could not be performed to determine quantitatively the specific surface area of the detectors. The Chronoamperometry measurement for two samples is reported in Figure 1f. The UV photo-response current (ΔI) and the recovery time were extracted from Figure 1f. The UV photoresponse current increases when comparing ZnO deposited on Glass and on the PAN electrospun nanofibers, which confirm the sweep voltammetry tests. Moreover the recovery time decreases. We should note that the UV photoresponse current has been enhanced by a factor of 24 (ratio between the ΔI of the PAN/ZnO 1D NSs electrode and the ΔI of the flat electrode) with an increase by a factor of 1.45 of the recovery time (ratio between the recovery time of the PAN/ZnO 1D NSs electrode and the recovery time of the flat

electrode). The latter should be considered negligible regarding the huge amount of current enhancement.

The photoconduction mechanism in a single ZnO nanowire has been studied by Wang *et al.*[34] In the dark, a depletion layer with low conductivity is created near the nanowires surface. This layer results from the adsorption of oxygen molecules on the nanowires surface as negatively charged ions by capturing free electrons from the n-type zinc oxide.
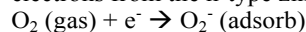
O_2 (gas) + e^- → O_2^- (adsorb)

Under UV illumination an electron-hole pair will be generated. Holes migrate to the surface and recombined with the O_2 species adsorbed on the surface through surface electron-hole recombination.

O_2^- (adsorb) + h^+ → O_2 (gas)
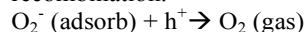
The unpaired electrons are collected at the anode under an applied voltage, which leads to an increase of the nanowire conductivity.

It is expected that increasing the surface area using the three-dimensional polyacrylonitrile /ZnO material may further enhance the sensitivity of the devices due to an increased surface to volume ratio. However, the recovery time will increase due to the long electron collection paths to the silver electrodes. In direct comparison, a flat Zinc oxide layer (without three-dimensional polyacrylonitrile materials) offers shorter electron collection paths.

2. Influence of the ZnO thickness on UV photodetection

In this section the influence of ZnO ALD thinckness is investigated. Supported PAN nanofibers with 240 seconds of electrospinning time have been used. Four different samples of ZnO with different numbers of ALD cycles were deposited on the PAN fibers: 250, 500, 750 and 1000 cycles which correspond to 50, 100, 150 and 200 nm thick ZnO respectively. All those samples were performed at 100°C. The ZnO film thicknesses have been calculated based on the growth per cycle for ZnO films observed elsewhere (GPA = 0.2 nm) (Table 1).[45, 47-54]
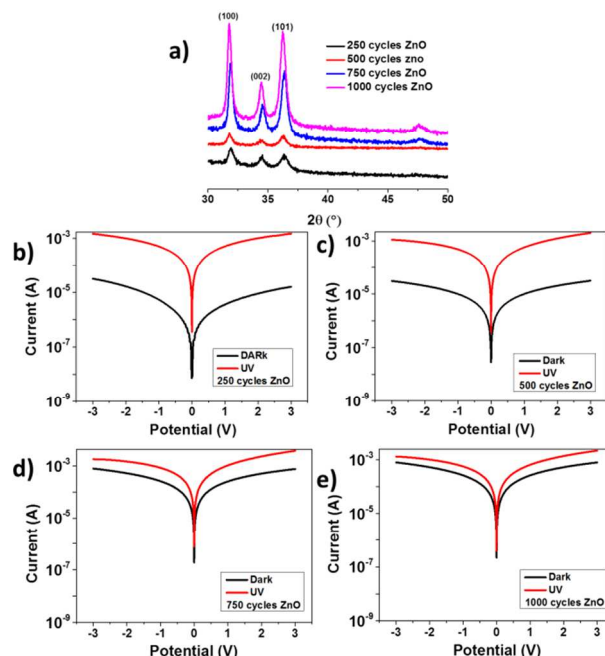
Figure 2. a) X-Ray diffraction spectra of 250, 500, 750 and 1000 cycles of ZnO deposited at 100°C; Sweep voltammetry of

50 (b), 100 (c), 150 (d), and 200 nm (e) ZnO ALD deposited on PAN NFs, in Dark and UV (365 nm).

Table 1. Thin films thicknesses and grain size calculation of ALD ZnO elaborated at 100°C with 250, 500, 750, and 1000 cycles; I_{UV} and I_{Dark} of different ZnO thicknesses with the I_{UV}/I_{Dark} current ratio at -1V bias; UV photoresponse current and the recovery time for the samples with different ZnO ALD thicknesses

Number of ALD cycles	250	500	750	1000
Films thicknesses (nm)	50	100	150	200
Grain size (nm)	18.30	23.01	25.05	25.90
I_{Dark} (A)	5.33×10^{-6}	9.90×10^{-6}	2.60×10^{-4}	2.62×10^{-4}
I_{UV} (A)	5.04×10^{-4}	5.34×10^{-4}	8.41×10^{-4}	5.60×10^{-4}
I_{UV}/I_{Dark}	94.50	53.90	3.23	2.13
ΔI (A)	5.70×10^{-4}	4.14×10^{-4}	2.90×10^{-4}	4.11×10^{-5}
UV photoresponse (A/W)	1.14×10^{-2}	8.2×10^{-3}	5.8×10^{-3}	8.2×10^{-4}
T (s)	144	985	763	162

XRD diffraction patterns of ZnO thin films are shown in Figure 2a. At 250 cycles ZnO, three weak peaks appear at $2\theta = 31.74°$, $34.42°$ and $36.22°$ respectively corresponding to (100), (002) and (101). Those three peaks become more intense at 750 and 1000 cycles ZnO. Moreover the XRD measurements show a preferred growth in the (100) direction. This preferred growth direction match the one reported for ZnO deposited on silicon substrate [45]. As shown in Table 1, the grain size increases from 18.3 nm to 25.9 nm with the number of ALD cycles (from 250 to 1000). This behavior was attributed to the columnar growth of the ZnO deposited by ALD. This increment on the grain size leads to a decrease in the specific surface. We note here that due to the high diameters of the PAN/ZnO 1D NSs (more than 300 nm), high resolution transmission electron microscopy observations could not be performred. Figure 2b-e shows the sweep voltammetry of the 50, 100, 150, 200 nm ZnO deposited by ALD on supported electrospun PAN fibers (240 s time) under dark and UV illumination at 365 nm. The sweep voltammetry of all ZnO sensors confirm an ohmic contact between the ZnO nanofibers and the Ag contact. In Table 1 are the reported I_{Dark}, I_{UV} and I_{UV}/I_{Dark} ratios for different ZnO at -1V bias. As shown on Table 1, the I_{UV} values are in the range of 10^{-4} A for whatever deposited ZnO thickness on PAN NFs. On the contrary the I_{Dark} increases (resistivity decreases) when the number of cycles rises. Due to this behavior under dark condition, the I_{UV}/I_{Dark} ratio decreases from 94.5 to 2.13 with the ZnO layer thickness. This result agrees with the ones reported by Tapily et al. [55]. This behavior can be attributed to the change in the amount of OH group in the ZnO ALD films. Indeed the latter decreases conversely to the ZnO layer thickness (as shown by the EDX results reported elsewhere).[45] The influence of the OH groups on the free carrier concentration was reported by Guziewicz et al. [56]. They demonstrate that the low fraction of OH group on the ALD ZnO layer leads to high free carrier concentration. In addition,

Liu et al. [57] demonstrates that a O_2 plasma treatment for ZnO can enhance the UV photoresponse due to the oxygen vacancies filling at the ZnO surface. This observation confirms the oxygen role on the UV photoresponse. We note here that due to their high resistivity, samples without ZnO ALD films or with ZnO thickness lower than 50 nm could not be tested.
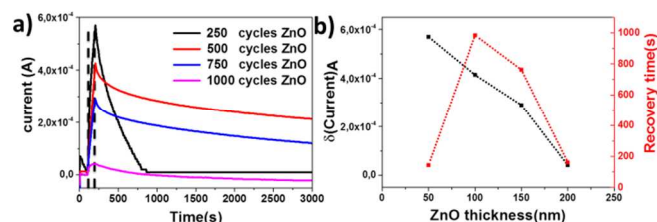

Figure 3. a) Chronoamperometry measurement for samples with different ZnO ALD thicknesses 50, 100, 150, and 200 nm deposited on PAN nanofibers with UV illumination (365 nm) 'on' between 100 and 200 s; b) UV photo-response current and recovery time versus ZnO ALD layer thicknesses.

The Chronoamperometry measurements for all samples are reported in Figure 3a. From these results, the UV photoresponse and the recovery time (Table 1) have been plotted against the ZnO ALD layer thicknesses (Figure 3b), in order to understand the influence of ZnO thickness on the UV photoresponse properties. The UV photoresponse current ΔI decreases conversely to the ZnO thickness due to the I_{Dark} increment. This can be due to the decrease on the amount of OH groups [56] as previously mentioned. In addition, it can also be related to the increase of the grain size with the ZnO thickness increases. That leads to a decrease on the specific surface of the ZnO sensor.[48] Despite the linear behavior of the photoresponse current, the recovery time shows two different performances: it rises with the thickness increases between 50 and 100 nm and then decreases between 100 and 200 nm. These uncharacteristic changes on the recovery time are not fully understood and could be related to the contact point between nanofibers. Aligned fibers spinning on a rotatory collector can be an interesting perspective to better illustrate this phenomena.

3. Influence of the PAN electrospinning time

The ZnO film with 50 nm (250 cycles) thickness has been used on the next part of this study due to its highest photoresponse current combined with the low recovery time. The specific sensors surface area can be controlled by the PAN electrospinning times. In order to investigate the influence of active surface on the UV photoresponse, five samples with different electrospinning times between 30 and 600 s were elaborated. A glass sample covered with a 50 nm ZnO layer without PAN nanofibers deposition has been used as reference. As shown by the SEM images (Figure 4a-d) the fiber density increases with the spinning time. Table 2 shows the I_{UV} and I_{Dark} with UV photoresponse current at -1V bias of different electrospinning times PAN fibers covered with 250 cycles of ALD ZnO.

The sweep voltammetry (figure 4 e-j) measurements exhibit a stable I_{Dark} value 10^{-5}-10^{-6} A at whatever electrospinning time (Table 2). On the contrary, the I_{UV} current increases from 2.26×10^{-6} to 4.01×10^{-3} A. This UV response increment was expected due to the enhancement on the specific area of the ZnO fiber exposed to UV light when the spinning time increases. This UV current increment leads to the increase of the ZnO detectors ΔI photoresponse from 2.15×10^{-5} to 3.91×10^{-3} A when the electrospinning time increases from 0 s to 600 s.
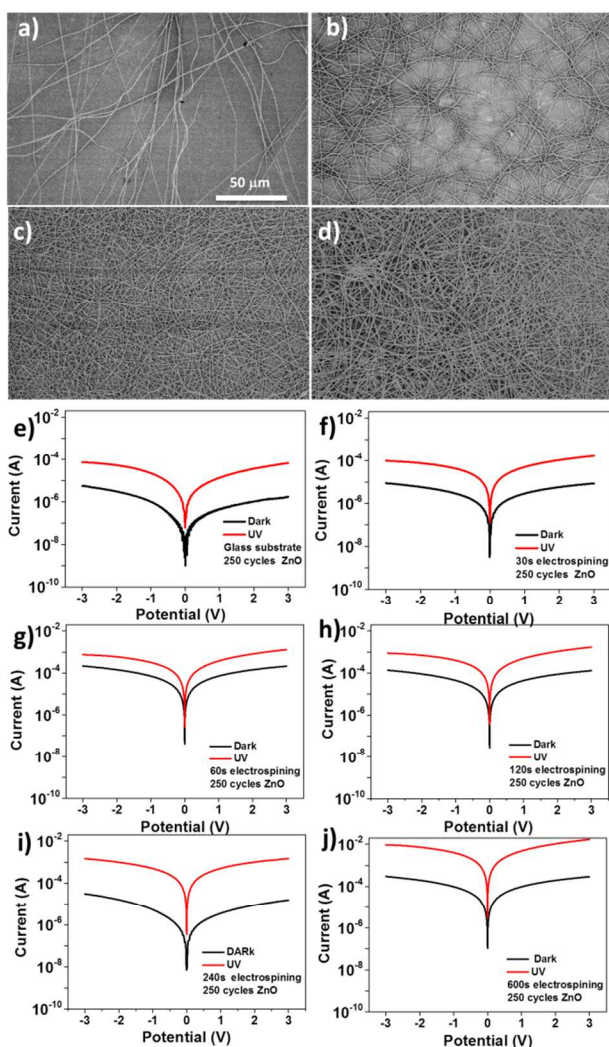
Figure 4. SEM images of PAN/ZnO 1D nanostructures obtained with different spinning times 30 (a), 60 (b), 240 (c), 600s (d); Sweep voltammetry of sensors with different electrospinning times 0 (e), 30 (f), 60 (g), 120 (h), 240 (i), and 600 s (j) in Dark and under UV (365 nm).

Table 2. I_{UV} and I_{Dark} with UV photoresponse current at -1V bias of different electrospinning time PAN fibers covered with 250 cycles of ALD ZnO; UV photoresponse current and the recovery time are also reported.

Electrospinning time (s)	0	30	60	120	240	600
I_{Dark} (A)	1.01×10^{-6}	2.91×10^{-6}	7.090×10^{-5}	4.48×10^{-5}	5.33×10^{-6}	9.88×10^{-5}
I_{UV} (A)	2.26×10^{-5}	4.31×10^{-5}	3.19×10^{-4}	4.00×10^{-4}	5.04×10^{-4}	4.01×10^{-3}
ΔI (A)	2.36×10^{-5}	4.21×10^{-5}	2.70×10^{-4}	2.53×10^{-4}	5.70×10^{-4}	6.07×10^{-3}
UV photoresponse (A/W)	4.7×10^{-4}	8.4×10^{-4}	5.4×10^{-3}	5.1×10^{-3}	1.14×10^{-2}	12.1×10^{-2}
T (s)	99	378	312	192	144	132

The UV photo-response current (ΔI) and the recovery times were extracted from Figure 5 and reported in Table 2, then plotted in Figure 5b versus the PAN electrospinning times. It allows illustrating the relation between the PAN electrospinning time and the UV photo-response properties. As shown in figure 5b, the UV photoresponse current increases with the PAN electrospinning time, which confirms the sweep voltammetry measurement. This behavior is related to the active surface enhancement. As discussed in the first section, increasing the surface area using the three-dimensional polyacrylonitrile /ZnO material may further enhance the sensitivity of the devices due to an increased surface to volume ratio.
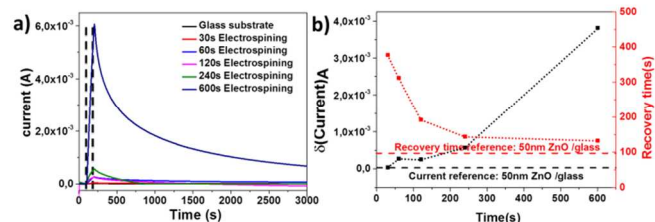

Figure 5. a) Chronoamperometry measurements of sensors with different electrospinning times 0, 30, 60, 120, 240, and 600 s with UV (365 nm) illumination between 100 and 200 s; b) UV photo-response current and recovery time versus PAN electrospinning time.

This behavior was also reported by Bai *et al.*[39]. The photoresponse current increases with the number of nanowires connected in parallel. Moreover the recovery time decreases conversely to PAN electrospinning time. The latter is induced by the increase of contact point number between the nanofibers with their amount. The recovery time will increase due to the long electron collection paths to the silver electrodes. Increasing the PAN electrospinning time enhances the UV photoresponse on both current and recovery time properties. We should note that the UV photoresponse current has been enhanced by a factor of 250 when the PAN electrospinning time (from 0 to 600 s) and an increase by a factor of 1.3 of the recovery time. The latter should be considered negligible regarding the huge amount of current enhancement.

4. UV characterization of ZnO ALD deposited at different temperatures

ZnO ALD deposition temperature effect was also investigated. Four different samples with ZnO ALD deposited at different temperatures between 50 and 130°C were investigated on 600 s PAN electrospinning time substrate. The thickness of the deposited ALD layer was 50 nm. As shown in Figure 6, XRD spectra at different temperatures 50, 80, 100 and 130°C shows three different peaks at $2\theta = 31.74°$, $34.42°$ and $36.22°$ respectively corresponding to (100), (002) and (101) matching the ZnO growth orientation reported elsewhere at 100°C on silicon substrate.[45] A change in the preferential growth orientation is observed when the deposition temperature increases from 50°C to 130°C. The preferred growth orientation changes from (100) to (101). Table 3 shows respectively the grain size (calculated from the equation 1) of 50 nm ZnO elaborated at 50, 80, 100 and 130°C. The grain size decreases when the ALD deposition temperature increases. Thus, the latter leads to increase the specific surface. This unexpected finding could be explained by the different ZnO nucleation behaviour on PAN nanofibers as the function of the

temperature involving different mechanism of precursor diffusion into the polymer.[51, 58]
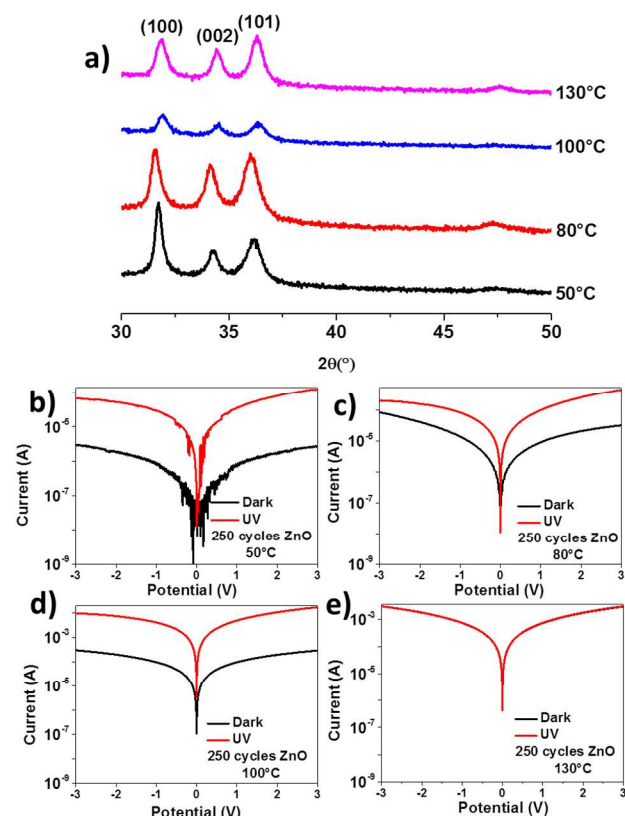

Figure 6. a) X-Ray diffraction spectra of 250 cycles ZnO elaborated at different temperatures between 50 and 130 °C; Sweep voltammetry of sensors with different deposition temperature; 50 °C (b), 80 °C (c), 100 °C (d), and 130 °C (e)

Table 3. Grain size values of 50 nm ALD ZnO elaborated at different temperatures 50, 80, 100 and 130°C. UV photoresponse current (ΔI) and recovery time (τ) of PAN/ZnO ALD with different temperatures.

ALD Temperature (°C)	50	80	100	130
Grain size (nm)	26.29	23.06	18.34	17.04
I_{Dark} (A)	7.86x 10^{-7}	1.40x 10^{-5}	9.62 x10^{-5}	7.41x 10^{-4}
I_{UV} (A)	2.92x 10^{-5}	8.41x 10^{-5}	3.99x 10^{-3}	7.46x 10^{-4}
ΔI (A)	1.80x 10^{-3}	3.34x 10^{-3}	6.06x 10^{-3}	-
UV photoresponse (A/W)	3.6 x10^{-3}	6.7 x10^{-3}	12.1 x10^{-2}	-
T (s)	138	480	132	-

Sweep voltammetry scans (Figure 6b-d) shows clearly that for the ZnO deposited between 50°C and 100°C, the UV illumination leads to a shift on the I(V) curve, on the contrary to the ZnO deposited at 130°C (Figure 6e). Moreover figure 6 shows an increase of I_{Dark} when the deposition temperature increases from 50 to 130°C. This behavior can be due to the OH group decreases when the deposition temperature increases

which lead to higher free carrier charge [56]. Similar results have been previously reported by Huby *et al.* [59] This increase of I_{Dark} leads to a negative behavior on the UV photoresponse. In addition, when increasing the deposition temperature, we decrease the grain size as reported in Table 3. This induces an increase of UV current as shown on Figure 5. The interference of those two opposite behaviors on the UV photoresponse leads to the highest UV photoresponse for the ZnO deposited at 100°C.
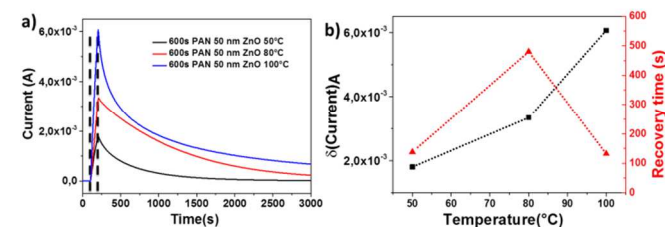
Figure 7. Chronoamperrometry measurement of PAN/ZnO ALD with different temperatures 50, 80, and 100°C with UV (365 nm) illumination between 100 and 200 s; b) UV photoresponse current and recovery time versus ZnO ALD deposition temperatures.
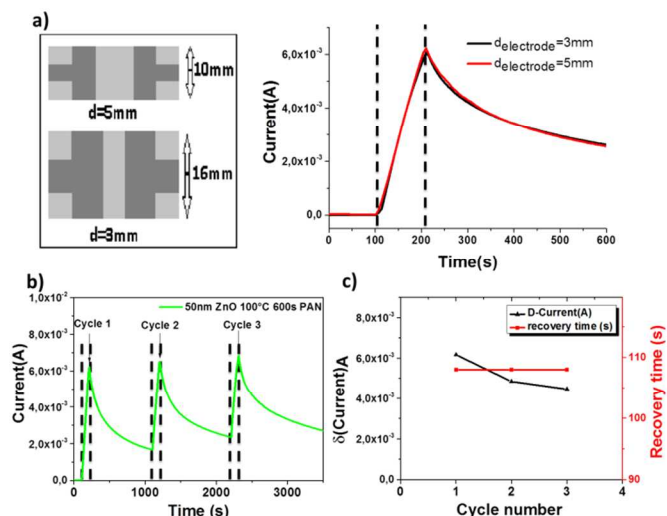
The UV photo-response current (ΔI) and the recovery time (τ) were extracted from chronoamperometry measurement (Figure 7a) and reported in Table 3. The data were plotted in Figure 7b versus the ALD deposition temperatures to investigate the relation between the ALD deposition temperature and the UV photoresponse properties. As shown in Figure 7b, the UV photoresponse current increases with ZnO ALD deposition temperature in the range between 50 and 100°C. The surface area increment (positive effect) characterized by the decreased of grain size with temperature overcomes the I_{Dark} increment (negative effect). On the contrary to the ZnO deposited at 130°C the I_{Dark} increment (negative effect) overcomes the active surface increment (positive effect) to lead to a zero photoresponse. Moreover an uncharacteristic change on the recovery time is observed. This behavior is not well understood for the moment. More experiments are in progress to better illustrate this phenomena.

5. Influence of ohmic contact distances and device stability

Samples with 600 s PAN electrospinning time and 50 nm ALD ZnO (250 cycles) at 100°C show the highest photo-response and the lowest recovery time (6.06 x10^{-3} A; 132 s). In order to study the effect of the distance between the electrodes, UV photoresponse tests were performed on the same type of sensor on larger substrate (16.5 mm) with nearest electrodes distance (3 mm) in order to keep the same working area (Figure 8a). Due to the nearest electrodes distance with the same illuminating area, the UV photoresponse current was approximately the same (6.17x10^{-3} A). In addition, the recovery time decreases from 132 to 108 s due the lower electron path between the electrodes that leads to faster discharge. This result was reported elsewhere by Prades *et al.*[40]. Shotcky contact can lead to lower recovery time due to the lower electron path between the electrodes. However, this type of contact cannot be achieved on the PAN nanofiber structure due to the high PAN nanofiber layer thickness.

Regarding the previous results, the stability of the sensor with 3 mm electrodes distance has been tested. Figure 8b shows the device stability test performed on this sensor. The UV photoresponse current and the recovery time was extracted from

Figure 8b and reported in table 4. Then it was plotted against the number of cycles on Figure 8c.

Figure 8. a) PAN/ALD ZnO sensor with different electrode distances; b) Device stability test of 600 s PAN electrospinning with 250 cycles ZnO at 100°C; c) UV photo-response current and the recovery time against the number of cycles.

Table 4. UV photoresponse current and recovery time of cycle 1, 2 and 3.

Cycle number	1	2	3
UV photo-response current (A)	6.17×10^{-3}	4.85×10^{-3}	4.47×10^{-3}
UV photoresponse (A/W)	12.3×10^{-2}	9.7×10^{-2}	8.9×10^{-2}
recovery time(s)	108	108	108

As shown in Table 4 and Figure 8c, the UV photoresponse decreases from 6.17×10^{-3} to 4.47×10^{-3} mA. This finding can be related to the non-total recovery of the I_{Dark} due to the insufficient time between the cycles (Figure 8). However, the recovery time remains constant for the 3 cycles.

A 50 cycles stability test has performed by increasing the cycle time in order to fully return dark current to its initial value. (see Supporting Information SI3). The test shows that the recovery time remains constant after 50 cycles however a decrease of UV photoresponse of about ~1.7%/cycle is observed. This decrease is not related to the technique used for the design of the UV sensor but to the well-known instability of ZnO under UV illumination. The UV illumination induces a change of the electrical properties and/or crystallinity of ZnO as has been reported elsewhere.[60]

Conclusions

In conclusion, by combining the electrospinning technique and the atomic layer deposition, ZnO 1D nanostructures have been synthesized and investigated as a UV photosensor. A significantly improved performance in the UV sensing has been observed. UV photoresponse current has been enhanced by a factor of 250 by comparing to flat glass substrate. An increase by a factor of 1.3 of the recovery time has been observed which is negligible versus the huge amount of current enhancement. Device stability tests show a small decrease on the UV photoresponse current with a constant recovery time after 3 UV on/off cycles.

We can conclude that the increase of the specific surface area of the electrode, which is provided by the network of the PAN NFs and the Atomic layer deposition conformal coating, is an efficient approach to improve the UV photoresponse current without losing the stability of the devices. The possibility of tuning the surface area, the conductivity, and the chemical composition should allow the applications of these nanostructured electrodes in other fields such as gas sensors, biosensing, photocatalytic, and photovoltaic applications.[50]

The technique we propose herein is versatile since it allows producing sensors with tailored properties. In fact the possibility to deposit different oxides materials by ALD (ZnO, SnO_2, TiO_2 etc.) and doped oxides[61] should allow designing UV and gas sensors with controlled sensitivity, signal-to-noise ratio, spectral selectivity, high speed and high stability.

Notes and references

[a] Institut Européen des Membranes, UMR 5635, ENSCM-UMII-CNRS, place Eugène Bataillon, 34095 Montpellier, France

Dr. Mikhael Bechelany, email. mikhael.bechelany@univ-montp2.fr, tel. 0033467149167

1.   X. Gu, G. Liu, M. Zhang, H. Zhang, J. Zhou, W. Guo, Y. Chen and S. Ruan, *Journal of Nanoscience and Nanotechnology*, 2014, **14**, 3731-3734.
2.   H. Huang, Y. Xie, Z. Zhang, F. Zhang, Q. Xu and Z. Wu, *Applied Surface Science*, 2014, **293**, 248-254.
3.   S. I. Inamdar and K. Y. Rajpure, *Journal of Alloys and Compounds*, 2014, **595**, 55-59.
4.   Z. Jin, L. Gao, Q. Zhou and J. Wang, *Scientific Reports*, 2014, **4**.
5.   D. Y. Kim, J. Ryu, J. Manders, J. Lee and F. So, *ACS applied materials & interfaces*, 2014, **6**, 1370-1374.
6.   A. Rostami, N. Ravanbaksh, S. Golmohammadi and K. Abedi, *International Journal of Numerical Modelling-Electronic Networks Devices and Fields*, 2014, **27**, 309-317.
7.   C.-Y. Tsay and S.-H. Yu, *Journal of Alloys and Compounds*, 2014, **596**, 145-150.
8.   L. van Schalkwyk, W. E. Meyer, J. M. Nel, F. D. Auret and P. N. M. Ngoepe, *Physica B-Condensed Matter*, 2014, **439**, 93-96.
9.   Y. Xie, L. Wei, Q. Li, Y. Chen, S. Yan, J. Jiao, G. Liu and L. Mei, *Nanotechnology*, 2014, **25**.
10. M. Zhang, G. Liu, X. Gu, J. Zhou, W. Guo, L. Shen and S. Ruan, *Journal of Nanoscience and Nanotechnology*, 2014, **14**, 3827-3830.
11. E. Munoz, E. Monroy, J. L. Pau, F. Calle, F. Omnes and P. Gibart, *Journal of Physics-Condensed Matter*, 2001, **13**, 7115-7137.
12. M. Y. Liao, Y. Koide and J. Alvarez, *Applied Physics Letters*, 2005, **87**.
13. E. Munoz, *Physica Status Solidi B-Basic Solid State Physics*, 2007, **244**, 2859-2877.
14. T. Toda, M. Hata, Y. Nomura, Y. Ueda, M. Sawada and M. Shono, *Japanese Journal of Applied Physics Part 2-Letters*, 2004, **43**, L27-L29.
15. E. Mollow, in *Photoconductivity Conference*, Wiley,1954; , New York, NY, USA,, 1954, p. 509.
16. G. M. Ali, C. V. Thompson, A. K. Jasim, I. M. Abdulbaqi and J. C. Moore, *Sensors*, 2013, **13**, 16801-16815.
17. H. S. Al-Salman and M. J. Abdullah, *Journal of Materials Science & Technology*, 2013, **29**, 1139-1145.

18. Z.-S. Hu, F.-Y. Hung, K.-J. Chen, S.-J. Chang, W.-K. Hsieh, T.-Y. Liao and T.-P. Chen, *Applied Surface Science*, 2013, **279**, 31-35.
19. S. Lee, S.-E. Ahn, Y. Jeon, J.-H. Ahn, I. Song, S. Jeon, D.-J. Yun, J. Kim, H. Choi, U. I. Chung and J. Park, *Applied Physics Letters*, 2013, **103**.
20. D. Li, Y. Meng, P. Zhang, Z. Liu and H. Zhao, *Japanese Journal of Applied Physics*, 2013, **52**.
21. J. C. Moore and C. V. Thompson, *Sensors*, 2013, **13**, 9921-9940.
22. J. Yu, C. X. Shan, X. M. Huang, X. W. Zhang, S. P. Wang and D. Z. Shen, *Journal of Physics D-Applied Physics*, 2013, **46**.
23. G. Li, J. Song, J. Zhang and X. Hou, *Solid-State Electronics*, 2014, **92**, 47-51.
24. S. Liang, H. Sheng, Y. Liu, Z. Huo, Y. Lu and H. Shen, *Journal of Crystal Growth*, 2001, **225**, 110-113.
25. C. Y. Liu, B. P. Zhang, Z. W. Lu, N. T. Binh, K. Wakatsuki, Y. Segawa and R. Mu, *Journal of Materials Science-Materials in Electronics*, 2009, **20**, 197-201.
26. M. Li, W. Anderson, N. Chokshi, R. L. DeLeon and G. Tompa, *Journal of Applied Physics*, 2006, **100**.
27. L.-W. Ji, C.-Z. Wu, C.-M. Lin, T.-H. Meen, K.-T. Lam, S.-M. Peng, S.-J. Young and C.-H. Liu, *Japanese Journal of Applied Physics*, 2010, **49**.
28. D. Jiang, J. Zhang, Y. Lu, K. Liu, D. Zhao, Z. Zhang, D. Shen and X. Fan, *Solid-State Electronics*, 2008, **52**, 679-682.
29. M. Li, N. Chokshi, R. L. DeLeon, G. Tompa and W. A. Anderson, *Thin Solid Films*, 2007, **515**, 7357-7363.
30. C. X. Shan, J. Y. Zhang, B. Yao, D. Z. Shen, X. W. Fan and K. L. Choy, *Journal of Vacuum Science & Technology B*, 2009, **27**, 1765-1768.
31. T. K. Lin, S. J. Chang, Y. K. Su, B. R. Huang, M. Fujita and Y. Horikoshi, *Journal of Crystal Growth*, 2005, **281**, 513-517.
32. S. J. Young, L. W. Ji, S. J. Chang and Y. K. Su, *Journal of Crystal Growth*, 2006, **293**, 43-47.
33. H. Kind, H. Q. Yan, B. Messer, M. Law and P. D. Yang, *Advanced Materials*, 2002, **14**, 158-+.
34. Z. L. Wang, *Materials Science & Engineering R-Reports*, 2009, **64**, 33-71.
35. J.-H. Huang, K. Zhang, N. Pan, Z.-W. Gao and X.-P. Wang, *Acta Physica Sinica*, 2008, **57**, 7855-7859.
36. C. S. Lao, M.-C. Park, Q. Kuang, Y. Deng, A. K. Sood, D. L. Polla and Z. L. Wang, *Journal of the American Chemical Society*, 2007, **129**, 12096-+.
37. S.-K. Tzeng, M.-H. Hon and I.-C. Leu, *Journal of the Electrochemical Society*, 2012, **159**, H440-H443.
38. M. H. K. Mamat, Z.; Zahidi, M.M.; Mahmood, M.R., *J. Appl. Phys.*, 2011, **6**.
39. S. Bai, W. Wu, Y. Qin, N. Cui, D. J. Bayerl and X. Wang, *Advanced Functional Materials*, 2011, **21**, 4464-4469.
40. J. D. Prades, F. Hernandez-Ramirez, R. Jimenez-Diaz, M. Manzanares, T. Andreu, A. Cirera, A. Romano-Rodriguez and J. R. Morante, *Nanotechnology*, 2008, **19**.
41. Y. H. Lin, P. S. Lee, Y. C. Hsueh, K. Y. Pan, C. C. Kei, M. H. Chan, J. M. Wu, T. P. Perng and H. C. Shih, *Journal of the Electrochemical Society*, 2011, **158**, K24-K27.
42. D. D. Lin, H. Wu and W. Pan, *Advanced Materials*, 2007, **19**, 3968-3972.
43. C. X. Shan, J. Y. Zhang, B. Yao, D. Z. Shen, X. W. Fan and K. L. Choy, *Journal of Vacuum Science & Technology B*, 2009, **27**, 1765-1768.
44. Z.-M. Huang, Y. Z. Zhang, M. Kotaki and S. Ramakrishna, *Composites Science and Technology*, 2003, **63**, 2223-2253.
45. A. Abou Chaaya, R. Viter, M. Bechelany, Z. Alute, D. Erts, A. Zalesskaya, K. Kovalevskis, V. Rouessac, V. Smyntyna and P. Miele, *Beilstein Journal of Nanotechnology*, 2013, **4**, 690-698.
46. M. Liao, L. Sang, T. Teraji, M. Imura, J. Alvarez and Y. Koide, *Japanese Journal of Applied Physics*, 2012, **51**.
47. A. Abou Chaaya, M. Le Poitevin, S. Cabello-Aguilar, S. Balme, M. Bechelany, S. Kraszewski, F. Picaud, J. cambedouzou, E. Balanzat, J.-M. Janot, T. Thami, P. Miele and P. Dejardin, *Journal of Physical Chemistry C*, 2013, **117**, 15306-15315.
48. A. Abou Chaaya, R. Viter, I. Baleviciute, M. Bechelany, A. Ramanavicius, Z. Gertnere, D. Erts, V. Smyntyna and P. Miele, *Journal of Physical Chemistry C*, 2014, **118**, 3811-3819.
49. S. Cabello-Aguilar, S. Balme, A. Abou Chaaya, M. Bechelany, E. Balanzat, J.-M. Janot, C. Pochat-Bohatier, P. Miele and P. Dejardin, *Nanoscale*, 2013, **5**, 9582-9586.
50. J. Elias, M. Bechelany, I. Utke, R. Erni, D. Hosseini, J. Michler and L. Philippe, *Nano Energy*, 2012, **1**, 696-705.
51. J. Elias, I. Utke, S. Yoon, M. Bechelany, A. Weidenkaff, J. Michler and L. Philippe, *Electrochimica Acta*, 2013, **110**, 387-392.
52. C. Marichy, M. Bechelany and N. Pinna, *Advanced Materials*, 2012, **24**, 1017-1032.
53. R. Raghavan, M. Bechelany, M. Parlinska, D. Frey, W. M. Mook, A. Beyer, J. Michler and I. Utke, *Applied Physics Letters*, 2012, **100**.
54. J. A. Whitby, F. Oestlund, P. Horvath, M. Gabureac, J. L. Riesterer, I. Utke, M. Hohl, L. Sedlacek, J. Jiruse, V. Friedli, M. Bechelany and J. Michler, *Advances in Materials Science and Engineering*, 2012.
55. K. Tapily, A. S. Raj, D. Gu, H. Baumgart and G. Rozgonyi, in *Physics and Technology of High-K Materials 8*, eds. S. Kar, S. VanElshocht, D. Misra, M. Houssa, D. Landheer and K. Kita, Electrochemical Soc Inc, Pennington, 2010, pp. 281-287.
56. E. Guziewicz, M. Godlewski, K. Kopalko, I. A. Kowalik, S. Yatsunenko, V. Osinnyi, W. Paszkowicz, E. Lusakowska and P. Dluzewski, *Journal of the Korean Physical Society*, 2008, **53**, 2880-2883.
57. M. J. Liu and H. K. Kim, *Applied Physics Letters*, 2004, **84**, 173-175.
58. B. Gong, Q. Peng and G. N. Parsons, *The Journal of Physical Chemistry B*, 2011, **115**, 5930-5938.
59. N. Huby, S. Ferrari, E. Guziewicz, M. Godlewski and V. Osinniy, *Applied Physics Letters*, 2008, **92**, -.
60. A. M. Soleimanpour, Y. Hou and A. H. Jayatissa, *Applied Surface Science*, 2011, **257**, 5398-5402.
61. M. Moret, A. Abou Chaaya, M. Bechelany, P. Miele, Y. Robin and O. Briot, *Superlattices and Microstructures*, 2014, **75**, 477-484.

TOC

We explored a new material with large surface area to enhance the performances of UV photodetector.

Journal of Materials Chemistry A Accepted Manuscript